

Symmetry and Explicit Marking of the Critical Phase in Two-Bath Spin-Boson Model

Yao Yao^{1,2}, Nengji Zhou^{3,4}, Javier Prior⁵, and Yang Zhao^{3*}

¹State Key Laboratory of Surface Physics and Department of Physics, Fudan University, Shanghai 200433, China

²Collaborative Innovation Center of Advanced Microstructures, Nanjing University, Nanjing 210093, China

³Division of Materials Science, Nanyang Technological University, Singapore 639798, Singapore

⁴Department of Physics, Hangzhou Normal University, Hangzhou 310036, China

⁵Departamento de Física Aplicada, Universidad Politécnica de Cartagena, Cartagena 30202, Spain

(Dated: April 18, 2021)

The spin-boson model is a paradigm for studying decoherence, relaxation, entanglement and other effects that arise in a quantum system coupled to environmental degrees of freedom. At zero temperature, a localization-delocalization phase transition is known to exist in the sub-Ohmic regime, where the standard density matrix renormalization group algorithm is inadequate due to the divergence in the number of low-frequency modes. This limitation is circumvented in this work by symmetrically optimizing the phonon basis and introducing an order parameter accounting for the U(1) symmetry for a two-bath spin-boson model, by which we are able to determine the classification and criticality of the phase transition explicitly. Compared with variational results, the critical phase is characterized by spontaneous vanishing of boson displacements in both the baths, resulting in an accurate phase diagram with three model parameters.

PACS numbers:

Introduction- Much attention has been devoted in recent years to optical properties of natural photosynthetic systems [1–4] and organic photovoltaic devices [5–10], where the quantum aspect of excitons and phonons is increasingly recognized to be essential in boosting the power conversion efficiency. In organic systems, e.g., delocalization of wave functions is found to be essential for the dissociation of excitons [5]. As an excitonic paradigm, a two-level system is described by a single spin one-half which is coupled to its phonon environment represented by boson modes. This leads to the celebrated spin-boson model (SBM) [11, 12], providing avenues to study the phase transition between the localized and delocalized phases, or from a slightly different perspective, the dynamical phase transition between the coherent and incoherent phases [13–22]. Despite its simplicity, the SBM is a highly nontrivial model in nearly all aspects, and currently contention still surrounds the existence and the precise locations of phase transitions. Designed to help understand intrinsic mechanisms of coherent exciton dynamics, every theoretical approach typically works accurately only in a certain applicable regime, which is far away from the critical point, preventing the method from addressing issues related to the phase transition.

The density matrix renormalization group (DMRG) is a powerful numerical technique to study the low-lying states in strongly coupled, one-dimensional systems [23]. Similar to that for the numerical renormalization group [24] method, the orthogonal polynomials theory can be employed to map the SBM to a one-dimensional chain with only nearest-neighbor coupling [25], allowing one to straightforwardly adapt the DMRG method to study the SBM with only model-free approximations. Over the last

few years, this approach has been extensively used for detailed studies of the phase transition of SBM [26–31]. Our recent work was devoted to the two-bath SBM (TBSBM) to investigate the phase transition in a comprehensive manner [30, 31]. We have also examined the dynamics of SBM with the time-dependent DMRG (t-DMRG) algorithm, compared it with two other established methods, and demonstrated that a unitary transformation for the state yields reliable, accurate results [32, 33].

The approach of the optimal phonon basis, originally developed to deal with coupled electron-phonon systems [34], is often adopted to reduce the dimension of the Fock space of bosons [28, 30]. Although it has been utilized for a variety of models [35–37], a serious problem arises in the context of the TBSBM wherein the symmetry is numerically broken and the analysis of the phase transition becomes obstructed [29]. In this work, we circumvent this problem by symmetrically optimizing the phonon basis and constructing numerics-friendly operators. Our approach is adapted specifically for the TBSBM such that the doubly degenerate ground states can be obtained in a credible manner, and properties of the phase transition can be studied with sufficient precision.

Model and methodology- We consider the TBSBM in which a single spin is coupled diagonally and off-diagonally to two independent baths characterized by continuum spectral densities. The corresponding Hamiltonian can be written as

$$\hat{H} = \sum_{\nu=z,x} \sum_l \left[\omega_l b_{l,\nu}^\dagger b_{l,\nu} + \frac{\sigma^\nu}{2} \lambda_{l,\nu} (b_{l,\nu}^\dagger + b_{l,\nu}) \right], \quad (1)$$

where σ^z and σ^x are the Pauli operators, $b_{l,\nu}^\dagger$ ($b_{l,\nu}$) is the creation (annihilation) operator of the l -th mode of frequency ω_l in the ν -th bath ($\nu = z, x$), and $\lambda_{l,\nu}$ represents the corresponding spin-bath coupling strength. In the traditional SBM, the bath spectral density has a cut-off

*Electronic address: YZhao@ntu.edu.sg

frequency ω_c . For simplicity, the same cut-off frequency is assigned to the spectral density functions of the two baths in this work, i.e., $J_\nu(\omega) = 2\pi\alpha_\nu\omega_c^{1-s}\omega^s e^{-\omega/\omega_c}$ with α_ν being the dimensionless coupling strength for the ν bath and s being the exponent. The case of $s < 1$ corresponds to the sub-Ohmic regime in which the localized, critical and delocalized phases have been claimed to exist [28]. We will focus on the sub-Ohmic regime due to its relevance and complexity.

As discussed earlier, the symmetry in the Hamiltonian (1) is of paramount importance to the numerical precision. To facilitate discussion, we introduce the operators

$$\mathcal{O}_z^\pm = \pm\sigma^z e^{i\pi\sum_l b_{l,x}^\dagger b_{l,x}}, \quad \mathcal{O}_x^\pm = \pm\sigma^x e^{i\pi\sum_l b_{l,z}^\dagger b_{l,z}}, \quad (2)$$

which commute with the Hamiltonian. Also of interest is their product, i.e.,

$$\mathcal{O}_y^\zeta = \mathcal{O}_z^\phi \mathcal{O}_x^\varphi = i\zeta\sigma^y e^{i\pi\sum_l (b_{l,x}^\dagger b_{l,x} + b_{l,z}^\dagger b_{l,z})}, \quad (3)$$

with $\zeta, \phi, \varphi = \pm$ following the common rule of products. Together with the identity operator \mathcal{I}^\pm , it can then be verified straightforwardly that the eight operators $\mathcal{I}^\pm, \mathcal{O}_z^\pm, \mathcal{O}_x^\pm, \mathcal{O}_y^\pm$ form a non-abelian group G , and its center is represented by $\{\mathcal{I}^\pm\}$. The factor group $G/\{\mathcal{I}^\pm\}$ is an abelian group whose irreducible representations are given by four one-dimensional ones, indicating the U(1) symmetry when $\alpha_z = \alpha_x$ [29]. On the other hand, the two-dimensional representation of the non-abelian group G , characterized by a nontrivial central extension of its factor group, participates in the decomposition in irreducible representations, resulting in the \mathbb{Z}_2 symmetry if $\alpha_z \neq \alpha_x$ [31]. Subsequently, eigenstates of the system and, the ground state in particular, are doubly degenerate, a novel feature that allows specifications of the numerical precision in dealing with the symmetry.

We thus proceed to develop the DMRG algorithm to deal with the highly symmetrical model. Widely used to study the SBM and related models [26–32], the DMRG approach starts with the discretization of the boson modes, and employs the orthogonal polynomials theory to represent the renormalized modes by a set of boson sites [25], with a transformed Hamiltonian

$$\tilde{H} = \sum_{\nu=z,x} \left[\sqrt{\frac{\eta_\nu}{4\pi}} \sigma^\nu (b_{0,\nu}^\dagger + b_{0,\nu}) + \sum_i \omega_i b_{i,\nu}^\dagger b_{i,\nu} + \sum_i (t_i b_{i+1,\nu}^\dagger b_{i,\nu} + \text{h.c.}) \right], \quad (4)$$

where η_ν is the renormalized coupling calculated from $\eta_\nu = \int_0^{\omega_c} J_\nu(\omega) d\omega$. Herein, ω_i and t_i are the frequency and the hopping integral for the i -th site of bosons, respectively, and the expressions for them can be found in Refs. [30–32].

Despite discretization of the spectral densities, the number of the bare phonon basis in the local Fock space for each renormalized boson mode is still infinite, hindering numerical calculations. A remedy is to truncate the

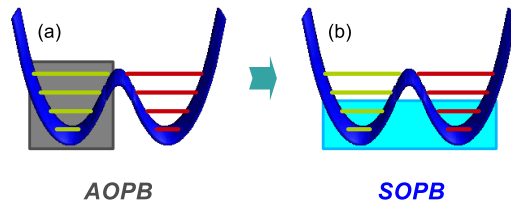


FIG. 1: Schematic for the two kinds of optimal phonon basis. (a) The AOPB is shown which takes into account the phonon bases with shifted displacements [28]. (b) The SOPB is shown which considers the globally lowest phonon bases.

Fock space and retain a finite number of bare phonon states for each mode, resulting in a so-called restricted phonon basis. Previous tests [32] reveal that the restricted basis method is applicable for the SBM away from the critical point, but fails to capture the phase-transition properties in the vicinity of the critical point. An approach employing an optimal phonon basis (OPB) was adopted by Zhang *et al.*, yielding improved results [34]. Details of the OPB-adapted DMRG algorithm can be found in the Supplementary Material. Numerical difficulties arise, however, in the OPB approach while correctly tackling the symmetry issues. A seemingly simple solution is to add an infinitesimal bias and to approach the critical point asymptotically. However, this would lead to a disastrously large difference in symmetry between $\alpha_z \neq \alpha_x$ and $\alpha_z = \alpha_x$ (the critical point) as discussed earlier. To circumvent this dilemma, we propose two techniques to enforce the model symmetry.

It is realized that in the implementation of the OPB approach, many low probability states are discarded. As sketched in Fig. 1(a), e.g., if the sign of the calculated boson displacement is negative, those states with a positive sign must be eliminated as they are almost orthogonal to the negative-displacement states. To recover the symmetry, therefore, the information in the eliminated states must be fed into the reduced density matrix, as depicted in Fig. 1(b). In particular, if $|g_i\rangle$ is the calculated ground state with i as the index of the left free site, we apply the parity operator $\mathcal{P}_i (\equiv e^{i\pi b_i^\dagger b_i})$ onto $|g_i\rangle$, obtaining $|g'_i\rangle$ with an opposite sign of the boson displacement on i -th site. This is numerically feasible as the i -th site is the one that has the Fock space based upon the bare phonon basis. With the two states obtained, the reduced density matrix of the i -th site is calculated by

$$\rho_i = \text{Tr}_E [a|g_i\rangle\langle g_i| + (1-a)|g'_i\rangle\langle g'_i|], \quad (5)$$

where Tr_E denotes the partial trace over all the sites except the i -th one and a is the portion of the state $|g_i\rangle$ in the reduced density matrix. In the absence of bias, it is intuitive to set a to 0.5. We then name the new basis obtained from the adapted reduced density matrix as the “symmetrically optimized phonon basis (SOPB),” and accordingly, the conventional OPB is called the “asymmetrically optimized phonon basis (AOPB).” We will show that the optimization procedure based on the SOPB

yields more accurate results.

With one run of the DMRG algorithm, one degenerate ground state is obtained, and with a second run, we may obtain another, allowing for a linear combination of the two [29]. However, symmetry breaking still persists reducing the accuracy and the efficiency. A sophisticated approach would then be to apply the operators (2) to the calculated ground state. In order to implement this operation, through the parity operator $\mathcal{P} \equiv \prod_i \mathcal{P}_i = e^{i\pi \sum_i b_i^\dagger b_i}$, a unitary transformation on all bosonic modes must be applied to flip the sign of displacements. As the bases of the boson modes have been symmetrically optimized, however, the number operator $\hat{n}_i \equiv b_i^\dagger b_i$ ceases to be diagonal. Moreover, the two degenerate states are almost orthogonal with each other, so that a simple diagonalization for \hat{n}_i can no longer guarantee numerical precision. In this context, we introduce a more numerically friendly treatment of the parity operator by recasting it in the form

$$\mathcal{P}_i = \sum_{n_i=\text{even}} |n_i\rangle\langle n_i| + \sum_{n_i=\text{odd}} e^{i\delta\theta} |n_i\rangle\langle n_i|, \quad (6)$$

where $|n_i\rangle$ is the eigenstate of the number operator \hat{n}_i at i -th site, and $\delta\theta$ is a small angle. Herein, following the t-DMRG algorithm [38], the angle π is divided into many small steps ($\delta\theta$) and the operator is applied incrementally to the ground state. The operator does not act on the even-number states, while for the odd-number states one can make $\mathcal{P}_i(\delta\theta)$ act cumulatively onto the state until a certain angle θ . If $\theta = \pi$ the action is equivalent to that of the parity operator, and if $\theta = 2\pi$ it is an identity operator. With this approach, reliable results can be obtained for all model parameters.

Results- In all the calculations we have carried out, the number of transformed bosonic site is set to be 50, the number of bare phonon basis is 16, and the DMRG truncating number is 64. Within these parameters, the error is reduced below 10^{-5} . The computation is time-consuming, e.g., on a single 2.13 GHz processor one run for a set of model parameters needs more than one hundred hours of CPU time.

We first discuss the deep sub-Ohmic regime with $s < 0.5$, in which a transition from localized to delocalized phases has been discussed in our previous work [30]. Fig. 2(a) shows $|\langle\sigma^z\rangle|$ and the ground-state energy E_g for various values of α_x with $s = 0.25$ and $\alpha_z = 0.02$. We compare three cases, with SOPB, with AOPB, and without any OPB adaption, and present results in the vicinity of the critical point. With $|\langle\sigma^z\rangle|$ plotted as a function of the α_x for the three cases and compared to our previous work [30, 31], a much sharper decrease of $|\langle\sigma^z\rangle|$ from a finite value to zero is found after the implementation of the parity symmetry. An α_x increment of 0.0002 is taken around the critical point, which is numerically equivalent to being infinitesimal. If the approach with SOPB gives rise to more precise results, it is implied that the phase transition here is more likely to be of first order. In addition, the ground-state energy is shown in the inset for

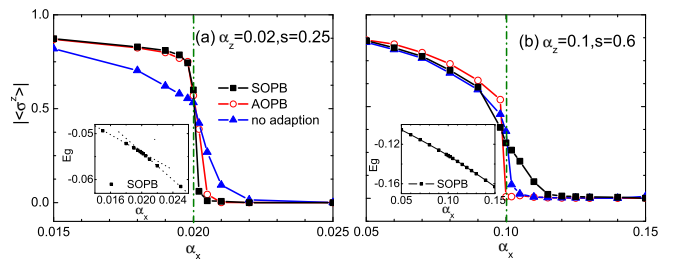


FIG. 2: $|\langle\sigma^z\rangle|$ versus α_x for three cases of the basis with (a) $s = 0.25, \alpha_z = 0.02$ and (b) $s = 0.6, \alpha_z = 0.1$. The green dash-dot lines indicate the phase boundary at $\alpha_x = \alpha_z$. The insets show the ground-state energy E_g versus α_x . The dotted lines in the inset of (a) are guides for eyes of the linear relationship.

the case with SOPB with the parity symmetry fully considered. It is observed that there is an obvious kink at the critical point implying the phase transition. To check the precision of the SOPB-adapted method, we show in the Supplementary Material the phase-angle dependence of the bosonic displacement, which serves as a measure of the precision. The results readily demonstrate the significant benefits accrued from the precision improvement.

The shallow sub-Ohmic regime with $0.5 \leq s < 1$ presents even richer physics. It has been claimed that when $s > 0.75$, there is a so-called critical phase at $\alpha_z = \alpha_x$ with $\langle\sigma^z\rangle$ and $\langle\sigma^x\rangle$ spontaneously vanishing [28]. From a mean-field analysis [31], however, a similar phenomenon is found for $s > 0.5$ instead of $s > 0.75$. The discrepancy may be attributed to the fact that the mean-field theory is valid in the weak-coupling limit, while previous DMRG calculations are applicable in the relatively strong coupling regime. To resolve the problem, it is necessary to work with a greater parameter space.

To this end, we first apply the SOPB-adapted approach to the case of $s = 0.6$. In Fig. 2(b), we display $|\langle\sigma^z\rangle|$ as a function of α_x obtained with SOPB, with AOPB and without OPB. It is found for the cases with AOPB and without OPB, $|\langle\sigma^z\rangle|$ shows a rather sudden change across the critical point. While adopting the SOPB method, the curve of the $|\langle\sigma^z\rangle|$ across the recognized critical point becomes much smoother as compared to the other two cases. This effect implies that the transition is of higher order than that with the deep sub-Ohmic bath. Moreover, the curve of the ground-state energy shown in the inset of Fig. 2(b) is also smooth close to the critical point.

In practice, merely considering the magnetization is insufficient to determine features of the phase transition. Derivation of a more explicit quantity with the complete information of both spin and baths is required for this purpose. The argument from the group theory shows that the operators (2) are the generators of the parity symmetry, with eigen-values of $+1$ or -1 . Following the group-theory argument, hereafter we calculate two quantities, $\langle\mathcal{O}_z\rangle$ and $\langle\mathcal{O}_x\rangle$, involving predictions of both the spin and the boson components. The calculation becomes

possible because, as tested, the action of the operator \mathcal{P} is precise based on the SOPB method.

For further clarity, we define an order parameter as $\zeta = \sqrt{\langle \mathcal{O}_z \rangle^2 + \langle \mathcal{O}_x \rangle^2}$. In the localized and delocalized phases with $\alpha_z \neq \alpha_x$, due to the orthogonality of the states $\mathcal{O}_x|g\rangle$ and $\mathcal{O}_z|g\rangle$, either $\langle \mathcal{O}_z \rangle$ or $\langle \mathcal{O}_x \rangle$ should be 1, such that the quantity ζ will always be unity. In the critical phase, as stated, the significance phenomenon is the spontaneous vanishing of $\langle \sigma^z \rangle$ and $\langle \sigma^x \rangle$, which obviously results in the vanishing displacements of bosonic modes. Let X and Z be the displacements of the bosonic mode in the two baths, respectively, which form a $X-Z$ plane for all the modes. The critical phase then refers to the case in which all the modes in the ground state are located at the origin of the $X-Z$ plane, indicating $\langle \mathcal{O}_z \rangle$, $\langle \mathcal{O}_x \rangle$ and ζ are all unity. Out of the critical phase, however, the continuous $U(1)$ symmetry dominates the critical point with $\alpha_z = \alpha_x$. It implies that the bosonic modes have certain displacements and deviate from the origin, leading to ζ smaller than one. The order parameter ζ accounting for the $U(1)$ symmetry is thus a measurement of the effective distance of this deviation.

Fig. 3(a) shows the α_x dependence of ζ with $\alpha_z = 0.02$ and 0.1 for $s = 0.25$ and 0.6, respectively. It is clear that for the deep sub-Ohmic case, ζ undergoes a sudden change between 1 and 0 close to the critical point ($\alpha_x = \alpha_z$). In terms of the above arguments, this finding proves the absence of a critical phase and clarifies the first-order phase transition for the sub-Ohmic bath. More interesting is the shallow sub-Ohmic case, in which ζ is between 0 and 1 at the critical point implying the possible appearance of the critical phase. In order to see the transition point between the localized and critical phases, we show in Fig. 3(b) the s -dependent ζ for five α_z 's right at $\alpha_x = \alpha_z$. It is found that ζ vanishes if s is small, while it becomes unity if s is larger than a certain value. More importantly, the larger the α_z , the larger the value of s for which ζ equals to one. In particular, for $\alpha_z = 0.1$, the transition point ζ becomes unity is lo-

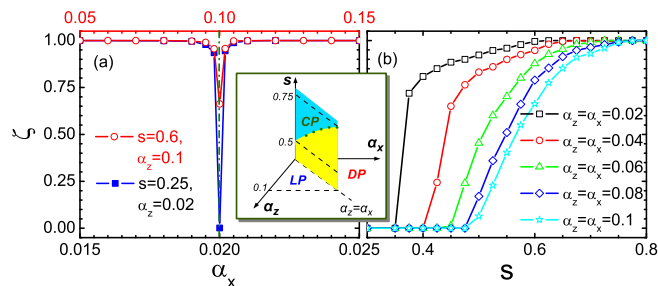


FIG. 3: (a) The order parameter ζ versus α_x changing from 0.015 to 0.035 for $s = 0.25, \alpha_z = 0.02$ and changing 0.05 to 0.15 for $s = 0.6, \alpha_z = 0.1$. The dash-dot line denotes the phase boundary. (b) ζ as a function of s for five sets of α_z and α_x . The inset shows the phase diagram consisting of the localized phase (LP), the delocalized phase (DP) and the critical phase (CP).

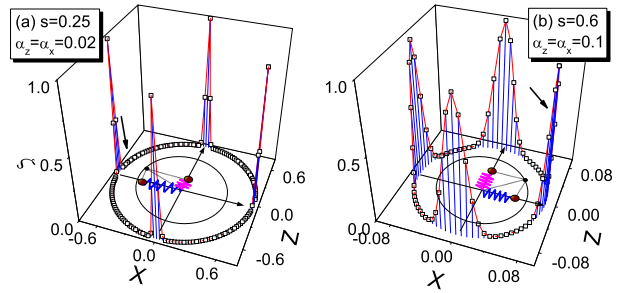


FIG. 4: The order parameter ζ calculated by the variational approach with rotational optimization shown in the $X-Z$ plane for (a) $s = 0.25, \alpha_z = \alpha_x = 0.02$ and (b) $s = 0.6, \alpha_z = \alpha_x = 0.1$. The radius of the circle in the $X-Z$ plane is determined by averaged boson displacements. The schematics in the $X-Z$ plane shows the displacements with respect to the calculated ground states, which are pointed out by the arrows as well.

cated at $s = 0.75$ which is in agreement with that of the previous work [28]. On the other hand, a scaling analysis of α_z to the weak-coupling limit shows the transition point of $\zeta = 1$ moving to $s = 0.5$ consistent with the expectation of the mean-field analysis [31]. Based on the transition points of ζ , we draw a phase diagram shown in the inset of Fig. 3, where the boundaries of the localized, delocalized and critical phases are explicitly determined.

Finally, to ensure that the vanishing ζ is not caused by numerical instability, we have also carried out the calculations based on variational theory [31]. Via this method, we first produce a state with the lowest energy, which is not necessarily the ground state especially at the critical point with high numerical noise. Afterward, we rotate the boson states with a phase angle Θ following the same procedure as that adopted for the DMRG calculations. This approach is justified because at the critical point the system obeys $U(1)$ symmetry. By comparing the energies of the states, a real ground state can be found subsequently. Details of this approach are provided in the Supplementary Material. For each state with Θ , we calculate the average displacements X and Z of both baths and the value of ζ accordingly, as shown in Fig. 4. To a large extent, ζ is also found to vanish by the variational approach, lending support to our DMRG results. More importantly, in the deep sub-Ohmic regime, ζ completely vanishes for a majority of the cases, implying the states to be almost orthogonal to each other. The location of the real ground state has been indicated by the arrows in Fig. 4, in agreement with the DMRG results. Moreover, we have also compared the average displacement of all the bosonic modes with the DMRG results and the results are presented in Supplementary Material. The displacement in the case $s = 0.6$ is much smaller than that of $s = 0.25$, implying the ground state of $s = 0.6$ to be closer to the origin of the $X-Z$ plane rather than that of $s = 0.25$. This finding elucidates why ζ is more likely to be nonzero for $s = 0.6$ than for $s = 0.25$.

Conclusion- In summary, we have employed the DMRG algorithm to study the TBSBM with both deep and shallow sub-Ohmic bosonic spectral densities. The numerical approach is adapted with the SOPB, and the parity operator is optimally constructed. It is found that through this adaptation, the numerical precision is greatly improved in both sub-Ohmic regimes. Using the SOPB method, we investigate the spin population and the ground-state energy. The results show that for $s = 0.25$ both the two quantities change significantly, supporting a feature of the first-order phase transition, while for $s = 0.6$ the changes become smoother indicating a higher order phase transition. We have also put forth a newly defined order parameter ζ , based on which

various features of the critical phase are discussed and the phase diagram is explicitly obtained. It is concluded that the SOPB-adapted DMRG algorithm is well-suited to handle the complexity of the phase transitions in the SBM. This robust approach is expected to be extended to tackle other issues, such as the real-time dynamics of the SBM.

acknowledgments- The authors gratefully acknowledge support from the NSF of China (Grant Nos. 91333202, 11134002 and 11104035), the National Basic Research Program of China (Grant No. 2012CB921401), and the Singapore National Research Foundation through the Competitive Research Programme (CRP) under Project No. NRF-CRP5-2009-04.

-
- [1] G. S. Engel, T. R. Calhoun, E. L. Read, T. K. Ahn, T. Mancal, Y. C. Cheng, R. E. Blankenship, and G. R. Fleming, *Nature (London)* **446**, 782 (2007).
- [2] I. P. Mercer, Y. C. El-Taha, N. Kajumba, J. P. Marangos, J.W. G. Tisch, M. Gabrielsen, R. J. Cogdell, E. Springate, and E. Turcu, *Phys. Rev. Lett.* **102**, 057402 (2009).
- [3] R. E. Fenna and B. W. Matthews, *Nature (London)* **258**, 573 (1975).
- [4] G. Panitchayangkoon, D. Hayes, K. A. Fransted, J. R. Caram, E. Harel, J. Wen, R. E. Blankenship, and G. S. Engel, *Proc. Natl. Acad. Sci. U.S.A.* **107**, 12766 (2010).
- [5] A. A. Bakulin, A. Rao, V. G. Pavelyev, P. H. M. van Loosdrecht, M. S. Pshenichnikov, D. Niedzialek, J. Cornil, D. Beljonne, and R. H. Friend, *Science* **335**, 340 (2012).
- [6] J. -L. Bredas, *Science* **343**, 492 (2014).
- [7] A. Rao, P. C. Y. Chow, S. Gélinas, C. W. Schlenker, C. Z. Li, H. L. Yip, A. K. -Y. Jen, D. S. Ginger, and R. H. Friend, *Nature (London)* **500**, 435 (2013).
- [8] S. Gélinas, A. Rao, A. Kumar, S. L. Smith, A. W. Chin, J. Clark, T. S. van der Poll, G. C. Bazan, and R. H. Friend, *Science* **343**, 512 (2014).
- [9] J. Guo, H. Ohkita, H. Bente, and S. Ito, *J. Am. Chem. Soc.* **132**, 6154 (2010).
- [10] S. M. Falke, C. A. Rozzi, D. Brida, M. Maiuri, M. Amato, E. Sommer, A. De Sio, A. Rubio, G. Cerullo, E. Molinari, and C. Lienau, *Science* **344**, 1001 (2014).
- [11] A. J. Leggett, S. Chakravarty, A. T. Dorsey, P. A. Fisher, A. Garg, *Rev. Mod. Phys.* **59**, 1 (1987).
- [12] U. Weiss, *Quantum Dissipative Systems*, 3rd ed. (World Scientific, Singapore, 2007).
- [13] D. Kast and J. Ankerhold, *Phys. Rev. Lett.* **110**, 010402 (2013).
- [14] R. Egger and C. H. Mak, *Phys. Rev. B* **50**, 15210 (1994); L. Mühlbacher, J. Ankerhold, *J. Chem. Phys.* **122**, 184715 (2005); L. Mühlbacher, J. Ankerhold, A. Komnik, *Phys. Rev. Lett.* **95**, 220404 (2005).
- [15] H. Wang and M. Thoss, *New J. Phys.* **10**, 115005 (2008); *Chem. Phys.* **370**, 78 (2010).
- [16] Z. Lü and H. Zheng, *J. Chem. Phys.* **136**, 121103 (2012).
- [17] A. Ishizaki and G. R. Fleming, *J. Chem. Phys.* **130**, 234111 (2009).
- [18] H. Hossein-Nejad and G. D Scholes, *New J. Phys.* **12**, 065045 (2010).
- [19] D. P. S. McCutcheon, N. S. Dattani, E. M. Gauger, B. W. Lovett, and A. Nazir, *Phys. Rev. B* **84**, 119903 (2011).
- [20] A. W. Chin, J. Prior, S. F. Huelga, and M. B. Plenio, *Phys. Rev. Lett.* **107**, 160601 (2011).
- [21] Y. Y. Zhang, Q. H. Chen, and K. L. Wang, *Phys. Rev. B* **81**, 121105(R) (2010).
- [22] P. Nalbach and M. Thorwart, *Phys. Rev. B* **81**, 054308 (2010).
- [23] S. R. White, *Phys. Rev. B* **48**, 10345 (1993).
- [24] R. Bulla, H. J. Lee, N. H. Tong, and M. Vojta, *Phys. Rev. B* **71**, 045122 (2005).
- [25] A. W. Chin, Á. Rivas, S. F. Huelga, and M. B. Plenio, *J. Math. Phys.* **51**, 092109 (2010).
- [26] J. Prior, A. W. Chin, S. F. Huelga, and M. B. Plenio, *Phys. Rev. Lett.* **105**, 050404 (2010).
- [27] C. Guo, A. Weichselbaum, S. Kehrein, T. Xiang, and J. von Delft, *Phys. Rev. B* **79**, 115137 (2009).
- [28] C. Guo, A. Weichselbaum, J. von Delft, and M. Vojta, *Phys. Rev. Lett.* **108**, 160401 (2012).
- [29] B. Bruognolo, A. Weichselbaum, C. Guo, J. von Delft, I. Schneider, and M. Vojta, arXiv:1410.3821 (unpublished).
- [30] Y. Zhao, Y. Yao, V. Chernyak, and Y. Zhao, *J. Chem. Phys.* **140**, 161105 (2014).
- [31] N. Zhou, L. Chen, Y. Zhao, D. Mozysky, V. Chernyak, and Y. Zhao, *Phys. Rev. B* **90**, 155135 (2014).
- [32] Y. Yao, L. Duan, Z. Lü, C. Q. Wu, and Y. Zhao, *Phys. Rev. E* **88**, 023303 (2013).
- [33] Y. Yao, *Phys. Rev. B* **91**, 045421 (2015).
- [34] C. Zhang, E. Jeckelmann, and S. R. White, *Phys. Rev. Lett.* **80**, 2661 (1998).
- [35] B. Friedman, *Phys. Rev. B* **61**, 6701 (2000).
- [36] A. Weiße, H. Fehske, G. Wellein, and A. R. Bishop, *Phys. Rev. B* **62**, R747 (2000).
- [37] W. Q. Ning, H. Zhao, C. Q. Wu, and H. Q. Lin, *Phys. Rev. Lett.* **96**, 156402 (2006).
- [38] A. J. Daley, C. Kollath, U. Schollwöck, and G. Vidal, *J. Stat. Mech.: Theor. Exp.* (2004) P04005; S. R. White and A. E. Feiguin, *Phys. Rev. Lett.* **93**, 076401 (2004).

Supplementary Materials: Symmetry and Explicit Marking of the Critical Phase in Two-Bath Spin-Boson Model

Yao Yao^{1,2}, Nengji Zhou^{3,4}, Javier Prior⁵, and Yang Zhao^{3*}

¹State Key Laboratory of Surface Physics and Department of Physics, Fudan University, Shanghai 200433, China

²Collaborative Innovation Center of Advanced Microstructures, Nanjing University, Nanjing 210093, China

³Division of Materials Science, Nanyang Technological University, 50 Nanyang Avenue, Singapore 639798

⁴Department of Physics, Hangzhou Normal University, Hangzhou 310036, China

⁵ Departamento de Física Aplicada, Universidad Politécnica de Cartagena, Cartagena 30202, Spain

(Dated: April 18, 2021)

PACS numbers:

I. OPTIMAL PHONON BASIS

The calculation procedure of the OPB-adapted DMRG algorithm, as sketched in Fig. 1, can be briefly summed up as follows. Firstly, we apply the usual DMRG procedure with restricted basis to obtain the state with the lowest energy which may be a rough estimate of the true ground state energy of the system [1]. To accelerate the computations, it is useful to add a very small bias ϵ to the system in this step to lift the degeneracy. The sign of the bias is not important in this step, because in the steps later on both degenerate states will be obtained and the influence of the small bias will be eliminated by the scaling analysis. Secondly, the DMRG iteration is continued, and the basis of the Fock space on the left single site is replaced by the bare phonon one during each step of the iteration. The number of bare basis (N_B) is much larger than that of the restricted basis (N_R), ensuring the con-

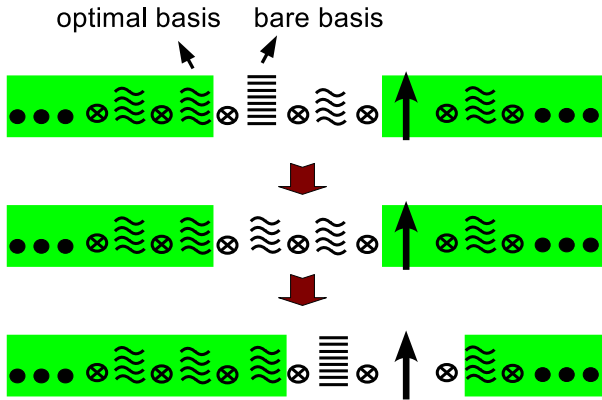


FIG. 1: Schematic for one step of the DMRG iteration with OPB. The left single site is initially with bare basis and the ground state is calculated for the whole system. Based upon the calculated state, the single site with bare basis is optimized. Following that the single site moves forward and the above step is redone. The large vertical arrow in the chain represents a spin.

vergence of the local energy. Thirdly, a new state with a much lowered energy with respect to the bare basis is obtained. Based upon this state, we calculate the reduced density matrix of the left single site and follow the idea of DMRG to discard those bases with low probability. The new reduced basis for the local Fock space is the OPB, carrying as much information as the bare phonon basis. After one iteration, all the boson sites are optimized with OPB, and then the system energy is minimized using the usual DMRG procedure. Finally, a state with an energy very close to that of the real ground state is obtained, with which we can calculate all desired observables.

II. EFFECTIVE DISPLACEMENT OF BOSONS

A. Deep sub-Ohmic regime ($s \leq 0.5$)

In order to examine the reliability of our numerical approach, we apply the operator $\mathcal{P}_i(\delta\theta)$ repeatedly onto the ground state $|g\rangle$ to obtain a new state $|\theta\rangle$. As discussed, the states with opposite displacements are orthogonal to each other, such that the new state with $\theta = \pi$ is orthogonal to the ground state, i.e., $\langle g|\theta = \pi\rangle = 0$. Therefore, if the information of the state with the opposite displacement is not taken into account in the procedure of the numerical optimization, the action of the operator $\mathcal{P}_i(\delta\theta)$ will give rise to results completely out of line with expectations. The examination of this operator is a critical criterion to determine whether our numerical approach is able to attain the double degeneracy, and thus the phase transition.

Based upon the state $|\theta\rangle$, we calculate the displacements of every boson mode $X_i(\theta) (\equiv 1/\sqrt{2}\langle b_i^\dagger + b_i \rangle)$ with both the symmetrically optimized phonon basis (SOPB) and asymmetrically optimized phonon basis (AOPB), and results shown in Fig. 2 are for the case of $\alpha_x = 0.02$ and 8 odd sites that are closest to the spin. It is found that with SOPB, displacements all switch signs when $\theta = \pi$, while the same signs are recovered when $\theta = 2\pi$. On the other hand, the AOPB displacements are found to be smaller than those of SOPB. More importantly, after a 2π rotation the displacements fail to return to their original positions, implying anomalies in the curves

*Electronic address: YZhao@ntu.edu.sg

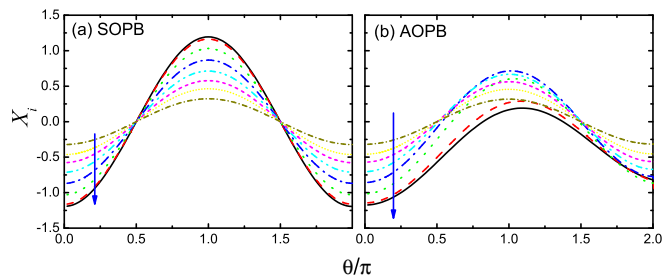


FIG. 2: The effective displacement of boson on the odd sites that are closest to the spin versus the rotation angle with (a) the SOPB and (b) the AOPB. The parameters are $s = 0.25$, $\alpha_z = \alpha_x = 0.02$, and $N_B = 16$. Different colours correspond to different sites, and the arrows indicate the orientation away from the spin.

when θ becomes large. We also calculate the energy (not shown), which is directly related to the displacement of the boson modes, and for the two cases we also observe that the energy of SOPB case at $\theta = 2\pi$ reproduces the original value while that of AOPB case does not. These results clearly show great improvements when the parity symmetry is explicitly taken into account. In addition, the deviation $|\Delta X_i|$ for the displacement of $\theta = 2\pi$ from that of $\theta = 0$ is a perfect measure of the numerical precision. The value of $|\Delta X_i|$ is found to be smaller than 10^{-5} in Fig. 2, indicating the results in the case of $s = 0.25$ and $\alpha_x = 0.02$ are reliable. We have also checked the value of $\langle g|\theta = \pi \rangle$ which is of the same order as the deviation.

B. Shallow sub-Ohmic regime ($0.5 < s < 1$)

In order to indicate the benefits of the SOPB method in the shallow sub-Ohmic regime, we show in Fig. 3 the phase angle dependence of the displacements for both SOPB and AOPB cases similar to that in the previous subsection. At variance to the deep sub-Ohmic case, the shallow sub-Ohmic bath produces no anomalies for the two bases, as the displacements show perfect rotations in line with the phase angle implying great precision. On the other hand, the AOPB method gives rise to much larger displacements than those from the SOPB method. Similar with the analysis in the deep sub-Ohmic case, a large displacement here would result in a large polarization of the spin, and the AOPB spin population shows a sudden change at the transition point, while the SOPB one shows a continuous crossover. The latter case is more accurate according to our previous mean-field analysis. Therefore, the applicable extent of the method is determined, that is, the SOPB-adapted method works well for both deep and shallow sub-Ohmic cases while dealing with the phase transition.

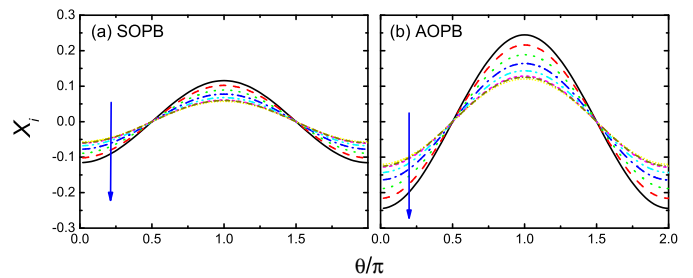


FIG. 3: The effective displacement of boson on the odd sites that are closest to the spin versus the rotation angle with (a) the SOPB and (b) the AOPB. The parameters are $s = 0.6$, $\alpha_z = \alpha_x = 0.1$, and $N_B = 16$. Different colours correspond to different sites, and the arrows indicate the orientation away from the spin.

III. THE VARIATIONAL APPROACH FOR THE TBSBM

A. The rotational optimization

In order to make a comparison, we adopt the variational approach [2] to calculate the quantities. The variational approach is based on the trial wavefunction

$$|\psi\rangle = |+\rangle \sum_n A_n \exp \left[\sum_l^{2M} \left(f_{n,l} b_l^\dagger - \text{H.c.} \right) \right] |0\rangle_{\text{ph}} + |-\rangle \sum_n B_n \exp \left[\sum_l^{2M} \left(g_{n,l} b_l^\dagger - \text{H.c.} \right) \right] |0\rangle_{\text{ph}}, \quad (1)$$

where $|+\rangle$ ($|-\rangle$) stands for the spin up (down) state in the Z -direction, H.c. denotes the Hermitian conjugate, $|0\rangle_{\text{ph}}$ is the vacuum state of the phonon bath, M and N represent the numbers of the bath modes and coherent superposition states, respectively, and $A_n, B_n, f_{n,l}$ and $g_{n,l}$ are the variational parameters. Herein, the variables n and l represent the rank of the coherent superposition state and the label of the bosonic mode, respectively. By defining the norm of the wave function as $D = \langle \psi | \psi \rangle$ and the energy E as $E = H/D$ with $H \equiv \langle \psi | \hat{H} | \psi \rangle$, one can derive the self-consistency equations as the variational conditions, namely

$$\frac{\partial H}{\partial \{\xi_i\}} - E \frac{\partial D}{\partial \{\xi_i\}} = 0, \quad (2)$$

where ξ_i denotes one of the variational parameters. The ground state is then searched by using this variational iteration technology.

Due to the numerical errors, however, the state $|\psi\rangle$ found by the variational approach may be a meta-stable state. This situation is quite similar to that in the DMRG calculation. In particular, since the coherent states are used as the trial wave function, the calculated critical point will always deviate from the theoretical point $\alpha_x = \alpha_z$. Motivated by the SOPB-adapted DMRG algorithm,

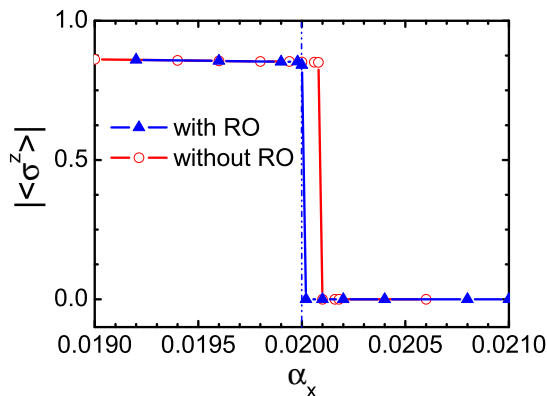


FIG. 4: $|\langle\sigma_z\rangle|$ calculated by the variational approach as a function of α_x ranging from 0.018 to 0.021 for $s = 0.25$ and $\alpha_z = 0.02$ with and without the rotational optimization (RO). The blue dash-dotted line indicates the critical point at $\alpha_x = \alpha_z$.

we then incorporate the symmetry into the variational approach. We construct a rotational operator $\hat{T}(\Theta) = \exp(i\Theta\hat{S})$, where

$$\hat{S} = \frac{1}{2}\sigma_y + i \sum_l (b_{l,x}b_{l,z}^\dagger - b_{l,x}^\dagger b_{l,z}) \quad (3)$$

is the generator of the U(1) symmetry. It is worth noting that, there is a hopping term between the two baths in the generator \hat{S} , making it hard to implement the U(1) symmetry in the DMRG algorithm which will be discussed later on. By applying the operator $\hat{T}(\Theta)$ onto the state $|\psi\rangle$, we are able to find the ground state with the lowest energy in the $X-Z$ plane, which is much more reliable than that found by the variational method without the optimization.

In the case with $\alpha_z = 0.02$ and $s = 0.25$, a sharp jump of the magnetization $|\langle\sigma_z\rangle|$ has been found at the critical point $\alpha_{x,c} \approx 0.02$, similar to the results obtained by the DMRG algorithm with SOPB. To locate the critical point explicitly, the behavior of the magnetization in a much narrower range $[0.019, 0.021]$ is investigated. As shown in Fig. 4, the value of the critical point $\alpha_{x,c} = 0.02000(1)$ is located with the rotational optimization, an improvement over $\alpha_{x,c} = 0.02008(1)$ obtained without the optimization, since the theoretical value of $\alpha_{x,c} = \alpha_z = 0.02$ is expected. It indicates that the rotational optimization makes the variational approach more precise in determining the critical point. Also calculated is the ground state energy E_g , as shown in Fig. 5. The slope of the curve $E_g(\alpha_x)$ is comparable with that obtained by DMRG, though the explicit value of E_g is slightly larger than that from DMRG, e.g., $E_g = -0.12917$ for the variational method and $E_g = -0.12923$ for the DMRG algorithm at $s = 0.6$ and $\alpha_x = \alpha_z = 0.1$, implying the high precision of the DMRG algorithm. Moreover, two distinct values of the slopes, 0.89 and 1.55, are obtained for the localized and delocalized phases, respectively, indicating a first order phase transition.

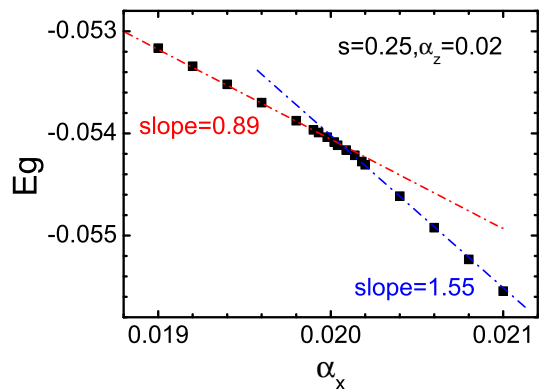


FIG. 5: The ground state energy E_g as a function of α_x at $s = 0.25$ and $\alpha_z = 0.02$ calculated by the variational approach with rotational optimization. The dashed lines represent the linear fits in both the localized (red) and delocalized phases (blue).

der phase transition.

B. Order parameter calculated by the variational approach with rotational optimization

The order parameter ζ is also calculated by the variational approach with the rotational optimization, in comparison with that from DMRG algorithm with SOPB. As shown in Fig. 6, ζ is plotted for the two cases of $s = 0.25, \alpha_z = 0.02$ and $s = 0.6, \alpha_z = 0.1$. In the deep sub-Ohmic regime with $s = 0.25 < 0.5$, ζ is found to be vanishing at the critical point $\alpha_x/\alpha_z = 1.0$, i.e., $\zeta(1.0) = 0$. On the other hand, a slight decrease from $\zeta = 1$ is found at the critical point in the shallow sub-Ohmic regime with $s = 0.6$. The result is in good agreement with that obtained by DMRG, indicating the potency of the SOPB-adapted DMRG algorithm.

To further understand the order parameter ζ at the

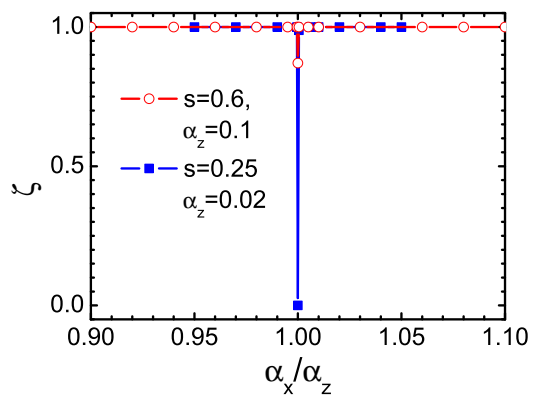


FIG. 6: The order parameter ζ calculated by the variational approach with the rotational optimization as a function of the ratio α_x/α_z for the two cases of $s = 0.25, \alpha_z = 0.02$ and $s = 0.6, \alpha_z = 0.1$, respectively.

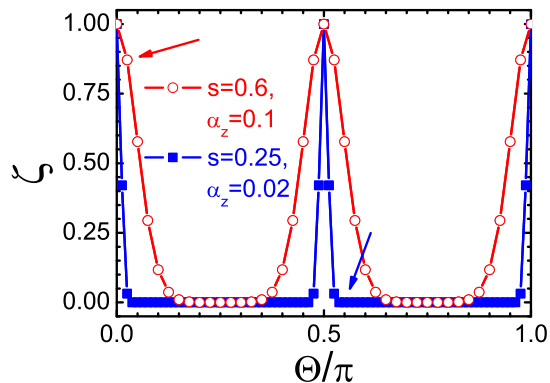


FIG. 7: The order parameter ζ calculated by the variational approach with the rotational optimization is displayed as a function of Θ/π for the two cases of $s = 0.25, \alpha_x = \alpha_z = 0.02$ and $s = 0.6, \alpha_x = \alpha_z = 0.1$ in the deep and shallow sub-Ohmic regimes, respectively. The arrows indicate the locations of the calculated ground states.

critical point, the behavior of $\zeta(\Theta)$ is investigated on the states $\hat{T}(\Theta)|\psi\rangle$ with the rotational optimization, as shown in Fig. 7. For $s = 0.25$ in the localized phase, sharp peaks of $\zeta(\theta)$ are found at $\Theta/\pi \approx n/2$ ($n = 0, 1, 2$) with a small peak width $\Delta\Theta_1$ defined as the size of the parity-symmetry regime with $\zeta > 0$. It suggests that the ground state is localized in a corner of the $X - Z$ plane, where X and Z corresponding to the diagonal and off-diagonal coupling baths, respectively. For $s = 0.6 > 0.5$ in the critical phases, the width of the peak $\Delta\Theta_2$ increases visibly. Interestingly, the ratio of these two peak widths $\Delta\Theta_2/\Delta\Theta_1 = 6.0$ is consistent with the ratio of ground state central angles being 6.3 in the $X - Z$ plane, indicating that the width of the peak is determined by the central angle. Since the ground state marked by the arrow is located nearby the peak, the value of ζ in the ground state increases with the width of the peak. It elucidates why ζ is more likely to be nonzero for $s = 0.6$ than that for $s = 0.25$ in Fig. 6.

IV. U(1) SYMMETRY OF TBSBM WITH SINGLE MODE

At $\alpha_x = \alpha_z$, the entire system obeys the U(1) symmetry with the generator expressed in Eq. (3). Very recently, Bruognolo *et al.* tried to incorporate the U(1) symmetry explicitly into the DMRG algorithm [3]. It is not easy done since there is a hopping term between the two bosonic baths in the generator. To implement the symmetry, they make a transformation in the Hamiltonian of TBSBM to mix the boson modes in the two baths. It is subsequently found that the approach does not work so well for the case of $s < 0.5$ due to the large truncation error. In comparison, our approach with SOPB can be applied to all cases, especially for the cases with $s < 0.5$ and $\alpha_z \neq \alpha_x$.

It was stated that in the numerical calculations the U(1) symmetry will always be broken spontaneously [3]. Indeed, our DMRG results do not show simultaneous magnetization disappearance in both Z and X orientations, i.e., $\langle \sigma^z \rangle = \langle \sigma^x \rangle = 0$. Whereas, the results of ζ show that the symmetry is still held. This shows that the involvement of the bosonic component in the order parameter is essential. To confirm this statement, we adopt the variational approach to investigate the system with two single-mode bosonic baths (i.e., $M = 1$ in Eq. (1)), which could be dealt with in a numerically exact manner. We will show that in the exact case, the symmetry is spontaneously broken in the strong coupling case with $\lambda \gg \omega$.

The ground state wave function of the TBSBM is also investigated to reveal the nature of the localized and delocalized phases. The phonon population $P(x, z)$ is introduced to describe the ground state of the two-bath model. Assuming that the wave function of the ground state can be written as

$$|\Psi_g\rangle = |+\rangle|\psi_+\rangle_{\text{ph}} + |-\rangle|\psi_-\rangle_{\text{ph}}, \quad (4)$$

where $|\psi_+\rangle_{\text{ph}}$ and $|\psi_-\rangle_{\text{ph}}$ are the phonon parts of the wave function corresponding to the spin up and down states, respectively, which can be expanded in a series of Fock states or coherent states. Thus the phonon population $P(x, z)$ is defined as

$$\begin{aligned} P(x, z) &= \langle \Psi_g(x, z) | \Psi_g(x, z) \rangle_{\text{spin}} \\ &= |\psi_+(x, z)|^2 + |\psi_-(x, z)|^2 \end{aligned} \quad (5)$$

where $\langle \dots \rangle_{\text{spin}}$ represents the trace of the spin freedom of the wave function, x and z correspond to the off-diagonal and diagonal coupling baths, respectively, and $\psi_{\pm}(x, z) = \langle \vec{r} | \psi_{\pm} \rangle_{\text{ph}}$ is the phonon part of the wave function in the two-dimensional coordinate representation $\vec{r} = (x, z)$.

According to the definitions of the phonon population $P(x, z)$ in Eq. (5) and the variational ansatz in Eq. (1), $P(x, z)$ can be calculated as

$$P(x, z) = \sum_{n=1}^N \frac{[A_n F_n(x, z)]^2 + [B_n G_n(x, z)]^2}{D}, \quad (6)$$

where $D = \langle \Psi_g | \Psi_g \rangle$ is the norm of the wave function, A_n and B_n denote the weight coefficients of the n -th coherent superposition state coupled to the spin up and down states, respectively, and $F_n(x, z) = \langle \vec{r} | \psi_+ \rangle_{\text{ph}} = f_{n,x}(x)f_{n,z}(z)$ and $G_n(x, z) = \langle \vec{r} | \psi_- \rangle_{\text{ph}} = g_{n,x}(x)g_{n,z}(z)$ represent the phonon part of the wave function $|\psi_{\pm}\rangle_{\text{ph}}$ in the coordinate representation $\vec{r} = (x, z)$. The function $f_{n,x}(x)$ denoting the phonon state in the off-diagonal coupling bath then can be obtained,

$$\begin{aligned} f_{n,x}(x) &= \prod_l \langle x | f_{n,l} \rangle \\ &= \prod_l \left(\frac{\omega_l}{\pi} \right)^{1/4} e^{-ix_l p_l / 2} e^{ip_l x} e^{-\omega(x-x_l)^2 / 2}, \end{aligned} \quad (7)$$

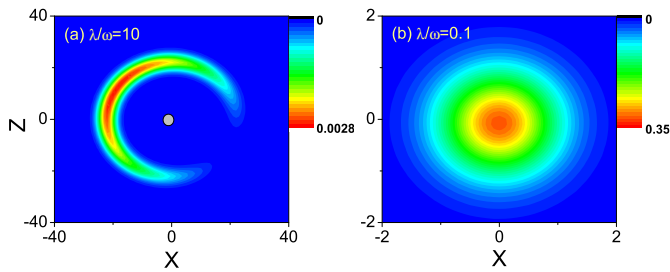


FIG. 8: The wave function of the ground state for the single-mode case (i.e., $M=1$ in Eq. (1)) is plotted in (a) for the strong coupling regime with $\lambda/\omega = 10$ and in (b) for the weak coupling regime with $\lambda/\omega = 0.1$. The X -coordinate and Z -coordinate correspond to the off-diagonal and diagonal coupling baths, respectively, and the colour represents the distribution of the phonon population $P(x, z)$.

where x_l and p_l are defined as

$$p_l = -i\sqrt{\frac{\omega_l}{2}} (f_{n,l} - f_{n,l}^*), \quad (8)$$

$$x_l = \frac{1}{\sqrt{2\omega_l}} (f_{n,l} + f_{n,l}^*). \quad (9)$$

In the same way, the functions $f_{n,z}(z)$, $g_{n,x}(x)$ and $g_{n,z}(z)$ can also be calculated from the displacement coefficients $f_{n,l}$ and $g_{n,l}$. Without loss of generality, we set the frequency ω_l to unity such that X and Z are now dimensionless. In the single-mode case with the number of effective bath modes $M = 1$, the function $F_n(x, z) = f_{n,x}(x)f_{n,z}(z) = \langle z|f_{n,1}\rangle\langle x|f_{n,2}\rangle$ is simplified, where the subscript 1 and 2 correspond to the diagonal and off-diagonal coupling baths, respectively.

As shown in Fig. 8 (a), the distribution of the phonon probability density $P(x, z)$ is located at a corner of the X - Z plane for the strong coupling regime with $\lambda/\omega = 10$, corresponding to the localized phase. Quite different from that in (a), the probability density distribution of the phonon $P(x, z)$ in the critical phase concentrates at the origin, as shown in Fig. 8 (b) for the weak coupling regime with $\lambda/\omega = 0.1$. It shows that the distance between the center of $P(x, z)$ and the origin is an important parameter to watch as one tells the localize phase from the critical one.

[1] S. R. White, Phys. Rev. B 48, 10345 (1993).

[2] N. Zhou, L. Chen, Y. Zhao, D. Mozysky, V. Chernyak, and Y. Zhao, Phys. Rev. B 90, 155135 (2014).

[3] B. Bruognolo, A. Weichselbaum, C. Guo, J. von Delft, I. Schneider, and M. Vojta, arXiv:1410.3821 (unpublished).